Phys. Lett. B 857 (2024) 138976

Contents lists available at ScienceDirect

Physics Letters B

journal homepage: www.elsevier.com/locate/physletb

Letter

Collectivity at the prolate-oblate transition: The 2_1^+ lifetime of ^{190}W

E. Şahin [a,b,c,*], V. Werner [a,c,*], A.K. Mistry [a,b,c], M. Rudigier [a], K. Nomura [d], J. Jolie [e], N. Pietralla [a], P.H. Regan [f,g], G. Ağgez [h], H.M. Albers [b], U. Ahmed [a,c], Ö. Aktaş [i], A. Algora [j,k], S. Alhomaidhi [a,b,c,l], C. Appleton [m], T. Arıcı [h], M. Armstrong [b,e], A. Banerjee [b], J. Benito [n], G. Benzoni [o], A. Blazhev [e], P. Boutachkov [b], A.M. Bruce [p], B. Cederwall [i], M.M.R. Chishti [f], M.L. Cortés [a,b], F. Crespi [o,q], B. Das [i], T. Davinson [m], T. Dickel [r], M. Doncel [s], A. Ertoprak [h,i], A. Esmaylzadeh [e], L.M. Fraile [n], E.R. Gamba [o,q], J. Gerl [b], M. Górska [b], J. Ha [t,u], E. Haettner [b], O. Hall [m], H. Heggen [b], C. Hornung [b], N. Hubbard [a,b,c], S. Jazrawi [f,g], P.R. John [a], C.E. Jones [p], V. Karayonchev [e], E. Kazantseva [b], R. Kern [a], L. Knafla [e], I. Kojouharov [b], P. Koseoglou [a], G. Kosir [v,w], D. Kostyleva [b], N. Kurz [b], N. Kuzminchuk [b], M. Llanos-Expósito [n], R. Lozeva [x], D. Mengoni [t,u], T.J. Mertzimekis [y], M. Mikolajczuk [b,z], A.I. Morales [j], I. Mukha [b], J.R. Murias [n], B.S. Nara-Singh [aa], S.E.A. Orrigo [j], J. Pellumaj [ab], S. Pelonis [ac], S. Pietri [b], S. Pigliapoco [t], Zs. Podolyák [f], M. Polettini [o,q], K. Rezynkina [t], H.A. Rösch [a,b], H. Schaffner [b], Ch. Scheidenberger [r,ad], L. Sexton [m], P.-A. Söderström [ae], Y.K. Tanaka [af], J.J. Valiente-Dobón [ab], P. Vasileiou [y], J. Vasiljević [i], J. Vesic [v], H. Weick [b], J. Wiederhold [a], A. Yaneva [b,e], G. Zhang [t,u], J. Zhao [b,ag], A. Zyriliou [y]

[a] Technische Universität Darmstadt, Institut für Kernphysik, D-64289 Darmstadt, Germany
[b] GSI Helmholtzzentrum für Schwerionenforschung, D-64291 Darmstadt, Germany
[c] Helmholtz Forschungsakademie Hessen für FAIR (HFHF), D-64289 Darmstadt, Germany
[d] Department of Physics, Hokkaido University, Sapporo, 060-0810, Japan
[e] Institut für Kernphysik, University of Cologne, D-50937 Cologne, Germany
[f] Department of Physics, University of Surrey, Guildford, GU2 7XH, UK
[g] Medical Marine and Nuclear Department, National Physical Laboratory, Teddington, Middlesex, TW11 0LW, UK
[h] Physics Department, Faculty of Science, Istanbul University, 34459 Vezneciler, Istanbul, Turkey
[i] Department of Physics, KTH Royal Institute of Technology, SE-10691 Stockholm, Sweden
[j] Instituto de Fisica Corpuscular, CSIC-Universidad de Valencia, E-46071, Valencia, Spain
[k] Institute of Nuclear Research, Debrecen H-4026, Hungary
[l] King Abdulaziz City for Science and Technology (KACST), P.O. Box 6086, Riyadh 11442, Saudi Arabia
[m] School of Physics and Astronomy, University of Edinburgh, Edinburgh, EH9 3FD, UK
[n] Grupo de Física Nuclear and IPARCOS, Universidad Complutense de Madrid, CEI Moncloa, E-28040, Madrid, Spain
[o] INFN Sezione di Milano, I-20133 Milano, Italy
[p] School of Computing, Engineering and Mathematics, University of Brighton, Lewes Road, Brighton, BN2 4GJ, UK
[q] Dipartimento di Fisica, Università degli Studi di Milano, Milano, Italy
[r] II. Physikalisches Institut, Justus-Liebig-Universität, Heinrich-Buff-Ring 16, D-35392 Gießen, Germany
[s] Department of Physics, Stockholm University, SE-10691 Stockholm, Sweden
[t] INFN Sezione di Padova, Padova, Italy
[u] Dipartimento di Fisica e Astronomia, Universitàt di Padova, Padova, Italy
[v] Jozef Stefan Institute, Jamova cesta 39, 1000 Ljubljana, Slovenia
[w] University of Ljubljana, Faculty of Mathematics and Physics, Jamova cesta 39, 1000 Ljubljana, Slovenia
[x] University Paris-Saclay, IJCLab, CNRS/IN2P3, F-91405 Orsay, France
[y] National & Kapodistrian University of Athens, Zografou Campus, Athens, GR-15784, Greece
[z] Faculty of Physics, University of Warsaw, Warsaw, 02093, Poland
[aa] SUPA, School of Computing, Engineering and Physical Sciences, University of the West of Scotland, Paisley, UK
[ab] INFN Laboratori Nazionali di Legnaro, Legnaro, Italy
[ac] KU Leuven, Instituut voor Kern- en Stralingsfysica, Leuven, Belgium
[ad] Helmholtz Research Academy Hesse for FAIR (HFHF), GSI Helmholtz Center for Heavy Ion Research, 35392 Giessen, Germany

* Corresponding authors.
E-mail addresses: e.sahin@gsi.de (E. Şahin), vw@ikp.tu-darmstadt.de (V. Werner).

https://doi.org/10.1016/j.physletb.2024.138976
Received 30 January 2024; Received in revised form 9 August 2024; Accepted 19 August 2024
Available online 22 August 2024

[ae] Extreme Light Infrastructure-Nuclear Physics, Horia Hulubei National Institute for Physics and Nuclear Engineering, Bucharest-Măgurele, Romania
[af] High Energy Nuclear Physics Laboratory, RIKEN, Wako, Japan
[ag] School of Physics, Peking University, Beijing 100871, China

ARTICLE INFO

Editor: B. Blank

Keywords:
Nuclear structure
γ-ray spectroscopy
Isomer spectroscopy
Shape phase transition
DESPEC
NUSTAR

ABSTRACT

The neutron-rich rare isotope ^{190}W is discussed as a candidate for a prolate-oblate transitional nucleus with maximum γ-softness. The collectivity of this isotope is assessed for the first time by the measurement of the reduced $E2$ transition probability of its first 2^+ state to the ground state. The experiment employed the FAst TIming Array (FATIMA), comprised of 36 $LaBr_3$(Ce) scintillators, which was part of the DESPEC setup at GSI, Darmstadt. The 4_1^+ and 2_1^+ states of ^{190}W were populated subsequently to the decay of its 127(12) μs isomeric $J^\pi = 10^-$ state. The mean lifetime of the 2_1^+ state was determined to be $\tau = 274(28)$ ps, which corresponds to a $B(E2; 2_1^+ \rightarrow 0_1^+)$ value of 95(10) W.u. The results motivated a revision of previous calculations within an energy-density functional-based interacting boson model-2 approach, yielding $E2$ transition properties and spectroscopic quadrupole moments for tungsten isotopes. From comparison to theory, the new data suggest that ^{190}W is at the transition from prolate to oblate structure along the W isotopic chain, which had previously been discussed as a nuclear shape-phase transition.

1. Introduction

In nuclear structure physics, the study of neutron-rich exotic nuclei plays a pivotal role in understanding the progression of nuclear shape towards exotic species. Radioactive ion beam facilities offer a way to experimentally study rare species. They have become increasingly significant in expanding our knowledge of the structure of exotic nuclei far from the β-stability line, and to probe predictions made on the base of stable nuclei, the alteration of which can inform us of new physics, such as the migration of magic numbers.

The ground states of neutron-rich nuclei in the A∼190 mass region exhibit an indication of shape evolution from a prolate to an oblate deformation [1,2]. Measuring the energy and lifetime of the first excited $J^\pi = 2^+$ state of even-even nuclei can provide first insights into the evolution of collectivity with neutron number [3–5]. More sensitive observables to the changes of structure are ratios of energies or transition strengths of low-lying states.

One such indicator is the ratio of the excitation energy of the 4_1^+ state to the first 2_1^+ state [$R_{4/2} = E(4_1^+)/E(2_1^+)$] [6]. This ratio is determined by the shape of the nucleus and can differentiate between an axially-symmetric deformed rotor with $R_{4/2} = 3.33$ and a spherical vibrational nucleus with $R_{4/2} = 2.0$, while it typically takes values of $R_{4/2} \sim 2.5$ for a triaxial rotor [7]. The stable even-even W isotopes with $106 \leq N \leq 112$ show values close to $R_{4/2} = 3.33$, implying a rigid axially-symmetric deformed shape. However, with the addition of more neutrons, the sudden reduction of the $R_{4/2}$ value to 2.73 in ^{190}W compared to the lighter isotopes, as indicated in Fig. 1, implies a shape change.

The landscape of nuclear deformation, spanning spherical, prolate, and oblate structures, is divided by shape transitional regions. These regions include soft rotors, where the level of "softness" varies depending on the β or γ (triaxial) degree of freedom. In fact, a collective phase diagram has been established [23], showing the separation of spherical vibrators from deformed nuclei by a first-order phase transition (β-soft rotors) [24–26], and a triple point of deformation (second-order phase transition) between spherical, prolate and oblate phases [27]. The oblate and prolate deformed nuclei are again separated by a first-order phase transition which corresponds to the limit of γ-soft rotors, where the nuclear potential is independent from the deformation parameter γ, which controls the triaxial degree of freedom. The prolate-oblate transition is most notably observed in the vicinity of $N = 90$, while γ-soft nuclei are commonly found in the corners of major nuclear shells. However, a prolate-oblate transition through γ-soft nuclei can be difficult to identify uniquely. Systematic investigations of basic observables have shown that nuclei in the region of $70 < Z < 78$ and $A \sim 190$ undergo the sought-after prolate-oblate phase transition. [3,4].

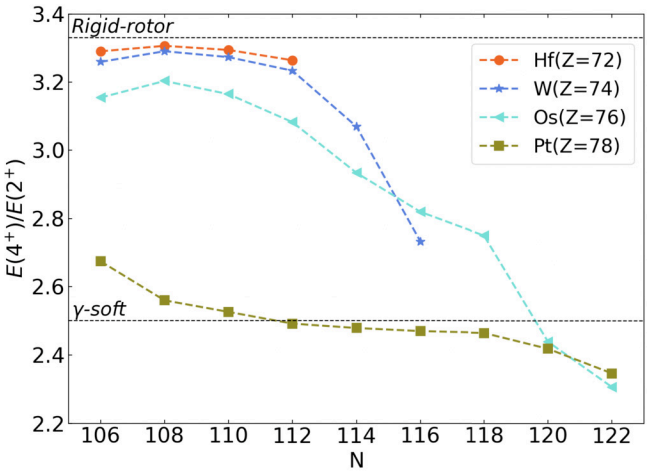

Fig. 1. The ratio $R_{4/2} = E(4_1^+)/E(2_1^+)$ for even-N Hf, W, Os and Pt isotopes. The data were taken from Nuclear Data Sheets and studies Ref. [8–22].

The neutron-rich nuclei in the W, Os, and Pt isotopes with mass numbers around $A \sim 190$ are the subject of various studies. Results indicate that the $R_{4/2}$ ratio in ^{190}W exhibits a sudden drop compared to the neighboring isotopes [28–33]. The experimental $R_{4/2}$ ratios of the lighter isotopes (Hf, W, Os) are close to the rotational limit, as shown in Fig. 1 (compare also Fig. 5 of Ref. [34]), and Pt isotopes around $N = 116, 118$ are well-known examples for nuclei close to the γ-soft limit [35]. The $R_{4/2}$ ratios then decrease toward heavier even-even isotopes with increasing neutron number. This decrease may be an indicator for γ softness, which is a well-established feature in this region [35–39], hence, potentially for the onset of the shape transition to oblate-deformed ground states [32,40,41]. Previous work on ^{188}W [41] yielded the heaviest isotopic $B(E2)$ value along the W elemental chain, toward neutron-rich nuclei. The rapid decrease in collectivity was discussed in terms of the development of γ softness, in line with theoretical calculations predicting that the maximum γ softness will occur at neutron number $N = 116$ in W and Os nuclei [32,4].

Different microscopic approaches generally agree with the development of (soft) triaxiality toward ^{190}W, however, they can give varying predictions on the nature of the shape transition. Examples range from a prolate-oblate shape-phase transition [32,42], over a rather smooth cross-over from prolate to soft triaxial and on to slightly oblate [43] and spherical structure [44], to the persistence of a prolate minimum, although with decreasing depth toward ^{190}W [45].

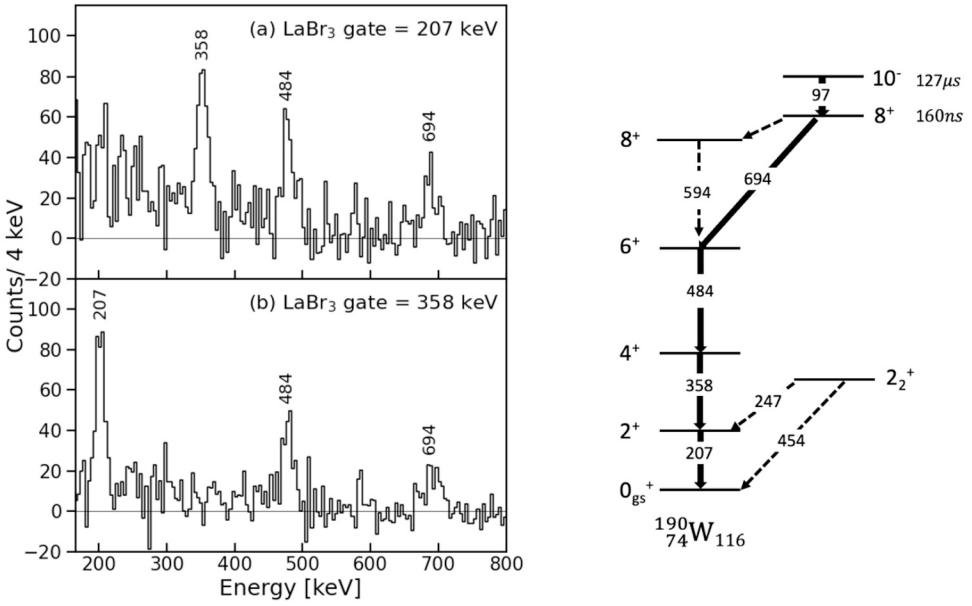

Fig. 2. The background subtracted $\gamma\gamma$-coincidence matrix for the long isomer ^{190}W was used to create projections. Two projections were created using $LaBr_3$(Ce) gates: (a) gate at 207 keV and (b) gate at 358 keV. The partial level scheme of interest is shown on the right, with dashed arrows marking unobserved transitions.

While the strongest experimental indicator of the shape transition in the W isotopes is, to date, based on excitation energies only, information on quadrupole collectivity from absolute transition strength in the most neutron-rich nuclei of this region is sparse but needed for a more firm characterization and analysis of the structural changes around $A = 190$.

In the present work, we report the first measurement of the quadrupole collectivity in terms of $E2$ properties for the $N = 116$ isotope ^{190}W. The measurement of the lifetime of the first-excited 2^+ state, hence, the reduced electric quadrupole transition probability $B(E2; 2_1^+ \rightarrow 0_1^+)$, extending the trend beyond ^{188}W for the first time, will allow new insights into the evolution of the nuclear shape in this region.

2. Experiment and data analysis

This study employed the DEcay SPECtroscopy (DESPEC) [46] setup at the Gesellschaft für Schwerionenforschung (GSI) at the final focal plane of the FRagment Separator (FRS). The experiment aimed to study heavy nuclear species produced via fragmentation reactions with a ^{208}Pb primary beam, which had an energy of 1 GeV/u and an intensity on the order of 10^8 ions per spill. The beam was directed towards a ^{9}Be target with a thickness of 2.7 g/cm^2. The ions of interest were separated from the produced fragments using the $B\rho$-ΔE-$B\rho$ technique and identified using the time-of-flight, $B\rho$, and ΔE technique by the FRS [47]. The experiment was carried out over approximately 8 days and the ions were implanted into the Advanced Implant Detector Array (AIDA) [46] located in the final focal plane of the FRS. The γ rays from the decay of excited states were detected using the FATIMA array consisting of 36 $LaBr_3$(Ce) scintillators [48], complemented by two EUROBALL cluster detectors positioned downstream, which served mainly to identify potential γ-ray contaminants to transitions of interest with high energy resolution.

For the analysis of γ rays and times, events within a range of the time after implantation and related deadtime of the system, ΔT, from 110 μs $\leq \Delta T \leq$ 1000 μs were accepted, and events in the range 1000 μs $\leq \Delta T \leq$ 2000 μs were used for background subtraction. A background-subtracted $\gamma\gamma$-energy coincidence matrix was created for the FATIMA array to analyze the coincidences between the observed γ rays for a $\gamma\gamma$-coincidence time window of 100 ns. Examples of gated spectra are shown in Fig. 2. Despite the limited statistics, the four γ-ray transitions detected by FATIMA occur in coincidence with each other. These data

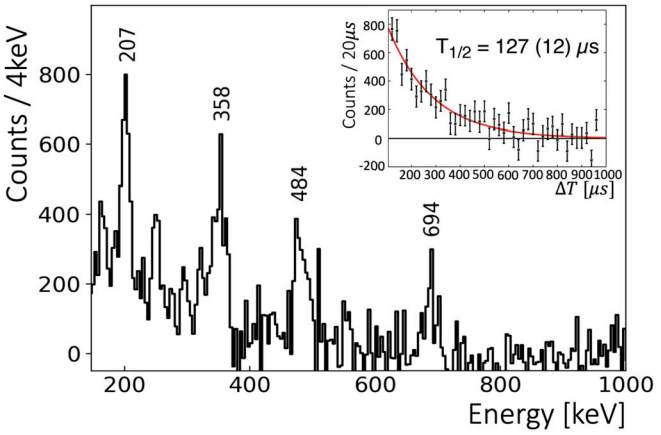

Fig. 3. Background subtracted FATIMA energy spectrum. In the inset, the $I^\pi = 10^-$ isomer decay curve with fit is shown.

corroborate that the observed transitions are indeed from sequential decays, in accordance with the level scheme established in Ref. [30]. Based on this pattern, the observed γ rays are following the decay of an 8^+ isomeric state, feeding the yrast $6_1^+ \rightarrow 4_1^+ \rightarrow 2_1^+ \rightarrow 0_1^+$ cascade.

The present experiment was sensitive to isomeric lifetimes in the micro-second range and the observed γ rays from ^{190}W showed a delayed time behavior, such that the half-life of an assumed isomeric feeding state could be determined by measuring the time difference ΔT between implantation and γ decay, i.e. between the S4 scintillator at the focal plane and FATIMA. A background-subtracted γ-ΔT matrix for the FATIMA array was created, and the total projection of the γ-ray energies is shown in Fig. 3. Fitted peak areas in time slices of 20 μs were then plotted as a function of time and fit by an exponential curve, as shown in the inset of Fig. 3. The half-life of the isomeric state in the present study was measured to be $T_{1/2}$ =127(12) μs from the 358-keV and the 484-keV transitions.

A previous high-resolution γ-ray study performed at GSI found that the $I^\pi = 10^-$ isomer in ^{190}W [34], originating from a neutron $K^\pi = 10^-$ $9/2^-[505]11/2^+[615]$ configuration, had a half-life of $T_{1/2}$ = 106(18) μs [29]. This half-life value was statistically compatible with the one of $T_{1/2}$ = 105(22) μs from an earlier experiment [49], however,

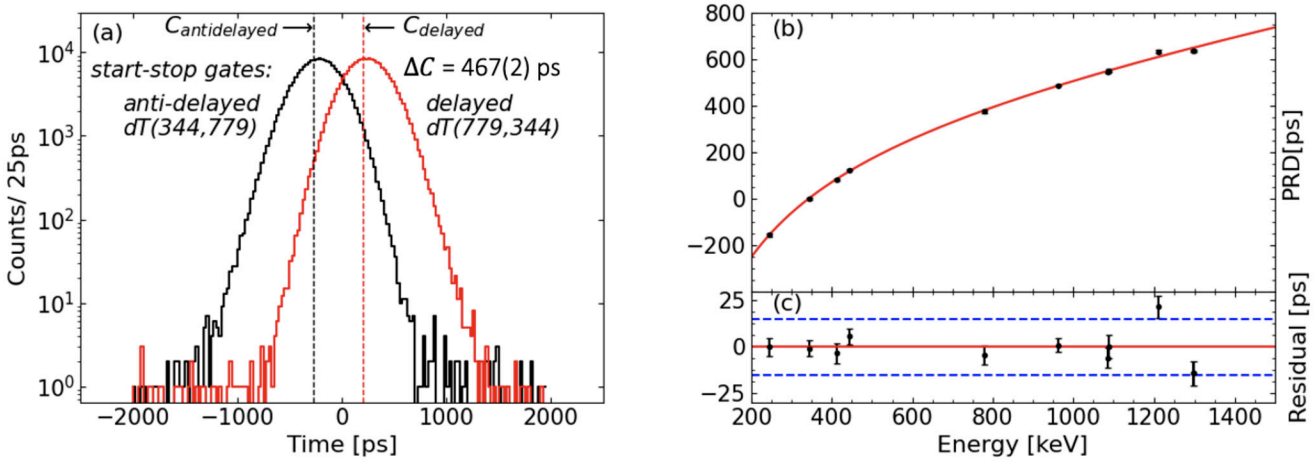

Fig. 4. (a) The delayed and anti-delayed time difference spectra of the decay cascade 779 → 344 keV were obtained by using coincidences with the 344 keV decay transitions in ^{152}Gd. (b) The PRD time-walk characteristics curve of the $\gamma-\gamma$ fast timing setup. (c) PRD residuals, i.e., the difference between the data and the fitted PRD function, the dashed lines represent two standard deviations (2σ).

at variance with the value of $T_{1/2} = 166(6)$ μs [30]. That work revealed that the 10^- isomer would not decay via the yrast 8^+ state, but a longer-lived 160 ns 8^+ isomeric state only 97 keV below the 10^- isomer.

The present experiment was not sensitive to the 97 keV transition nor to an intermediate state with a 160 ns lifetime, which is well within the uncertainty of the feeding μs isomer's lifetime. Nevertheless, the present isomer half-life of 127(12) μs supports the previous values derived at GSI over the value of Ref. [30]. The latter, however, used a different production mechanism which may have led to different populations of initial states. We further note that due to the long correlation time window of 2 ms and the subtraction of random background in the present lifetime measurement the decay curve shown in Fig. 3 clearly approaches zero, which has not been the case in the previous studies, which were limited to a range of few hundred microseconds.

The time resolution of the FATIMA setup greatly influences the accuracy of the fast-timing technique. In order to optimize the technique, the time distributions of the $LaBr_3$(Ce) detectors must be aligned before applying a time walk correction and carrying out the lifetime analysis. This was accomplished by using γ-ray transitions from a ^{60}Co source, and the time resolution at ^{60}Co energies, measured with VME electronics, is 320 ps (see Ref. [46]).

The fast-timing technique, which is introduced in [50,51], was utilized to determine the lifetime of the first excited state of ^{190}W on a picosecond range. If the lifetime of the nuclear state is shorter than the time resolution of the prompt distribution, also known as the "Prompt Response Function (PRF)", the Generalized Centroid Difference Method (GCD) [52,53] offers a reliable way to determine the lifetime. This technique is based on the centroids of time distributions between the "feeder" and "decay" transitions of the excited state, which act as start and stop signals, and vice versa, using a three-dimensional $E_{\gamma1} - E_{\gamma2} - \Delta T$ matrix (cube).

Time distributions $D(t)$ result from folding the PRF with an exponential function and are experimentally obtained. The centroid of $D(t)$ is then given by [54,55]

$$C(D) = < t > = \frac{\int_{-\infty}^{\infty} t D(t)\, dt}{\int_{-\infty}^{\infty} D(t)\, dt}. \quad (1)$$

The choice of the time start from the feeding (de-exciting) γ-ray defines delayed (anti-delayed) time distributions. The time difference between the centroids of the delayed (C_d) and anti-delayed (C_a) time distributions,

$$\Delta C = C_d(D) - C_a(D), \quad (2)$$

is related to the mean lifetime τ through [56]

$$\tau = \frac{1}{2}[\Delta C - PRD(E_{feeder}, E_{decay})], \quad (3)$$

where the Prompt Response Difference $PRD(E_{feeder}, E_{decay}) = C_d(P) - C_a(P)$ is the difference between the centroids of delayed and anti-delayed PRFs at the respective energies. The PRD function is used to describe the time-walk behavior of the two-timing branches in the detector setup. The centroid shift difference between the delayed and anti-delayed time distributions is shifted by $+2\tau$ from the corresponding PRD curve. In order to obtain a walk-free reference timing signal, an energy-dependent PRD curve is fit to γ-ray coincidence data from the decays of a ^{152}Eu source populating states with well-known lifetimes (see Fig. 4). In particular, we find $PRD(358, 207) = 255(5)$ ps.

To measure the lifetime of the 2_1^+ state of ^{190}W, a background-subtracted three-dimensional $E_{\gamma1} - E_{\gamma2} - \Delta T$ matrix was used to apply the GCD method. Similarly to the above, the time background was selected from the region 1000 μs $\leq \Delta T \leq$ 2000 μs. In addition, a $\gamma\gamma$ energy coincidence condition was applied on the feeder-decay cascade ($E_{\gamma1}$,$E_{\gamma2}$) corresponding to a given state of interest to the $E_{\gamma1} - E_{\gamma2} - \Delta T$ matrix. As a result of these steps, the delayed and anti-delayed time difference spectra were generated between a start and a stop detector, which were then used for the lifetime analysis.

Time differences between the feeding transition at $E_{feeder} = 358$ keV, ($4_1^+ \rightarrow 2_1^+$), and the decay transition at $E_{decay} = 207$ keV, ($2_1^+ \rightarrow 0_1^+$), have been projected from gates on the $\gamma\gamma$-coincidences. The resulting time distributions are shown in Fig. 5. No significant time-correlated Compton background events underneath the peaks of interest were observed. The analysis of the delayed and anti-delayed centroid difference resulted in a value of $\Delta C = 803(56)$ ps. Using this information and the formula in Eq. (3), the mean lifetime was determined to be $\tau = 274(28)$ ps, i.e., corresponding to a half-life of $T_{1/2} = 190(19)$ ps.

The same methods described above were used to derive the mean lifetime of the 4_1^+ state, τ_{4^+}. Due to limited statistics and the given time resolution of the setup we were only able to extract an upper limit of $\tau_{4^+} < 28$ ps at a 95.4% confidence level.

3. Discussion

From the measured mean lifetime of the 2_1^+ state of ^{190}W and the electron-conversion coefficient $\alpha = 0.276(4)$ from [57], we determine its reduced quadrupole transition strength to the ground state to $B(E2; 2_1^+ \rightarrow 0_1^+) = 95(10)$ W.u. This value clearly indicates quadrupole collectivity and motivates its discussion in terms of respective collective nuclear models. In the following, we will discuss our result in view of the shape evolution of the tungsten isotopes. Furthermore, we can base the discussion on calculations within an EDF-IBM-2 approach using the

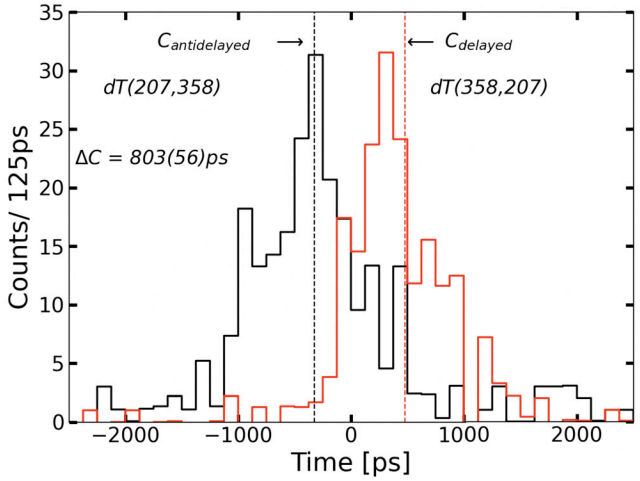

Fig. 5. (a) Delayed (red) and anti-delayed (black) time distributions generated from the $4_1^+ \rightarrow 2_1^+ \rightarrow 0_1^+$ cascade in ^{190}W.

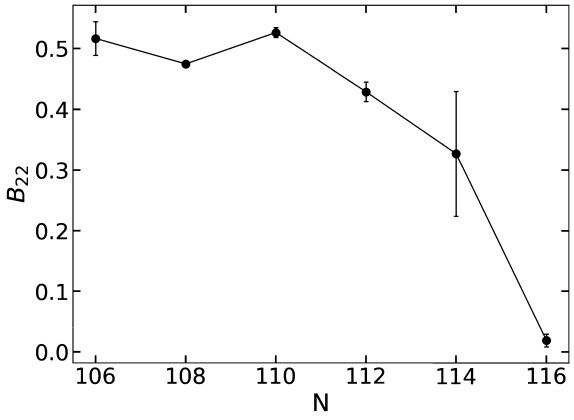

Fig. 6. The B_{22} ratio as a function of neutron number for the tungsten isotopic chain. Data taken from Refs. [8,11–14].

formalism which has been introduced for the structural analysis of Os and W isotopes [32].

The $R_{4/2}$ values in the W isotopic chain have already been shown in Fig. 1 and discussed further above, showing a drop toward ^{190}W at $N = 116$, to a value of $R_{4/2} \approx 2.6$, typical for a γ-soft nucleus. Such an energy ratio could also occur in other structural regions, however, the low energy of the 2_2^+ state below the 4_1^+ state corroborates the interpretation near the γ-soft limit. Furthermore, the ratio $B_{22} = B(E2; 2_2^+ \rightarrow 0_1^+)/B(E2; 2_2^+ \rightarrow 2_1^+)$, shown in Fig. 6, is diminishing toward ^{190}W. Such near-forbidden decay of the 2_2^+ state to the ground state is also typical for nuclei approaching the γ-soft limit [58], where it resembles the selection rule $\Delta v < 2$ for $E2$ transitions with respect to the $O(5)$ seniority quantum number v. Note that significant $M1$ strength from the second-excited 2^+ state is unlikely, and for $^{182-188}$W, the $2_2^+ \rightarrow 2_1^+$ transition is known to be of nearly pure $E2$ character, which we therefore also assume for ^{190}W.

Fig. 7(a) shows $B(E2; 2_1^+ \rightarrow 0_1^+)$ values for the Hf, W, Os and Pt isotopes from literature and the newly-derived value from the present work. All data are systematically down-sloping from the mid-shell region toward the $N = 126$ shell closure. Considering the larger uncertainties for the neutron-rich ^{188}W and ^{190}W, the new data point for ^{190}W extends the trend from $^{176-188}$W and is, within the experimental uncertainty, in agreement with a systematic drop of $B(E2)$ values as a function of neutron number. However, there is an indication for a potentially flat behavior from $N = 114$ to $N = 116$, which is discussed within the theoretical framework below.

The $B(E2)$ values up to ^{190}W can now be compared to theoretical predictions. On an absolute scale, the results from Ref. [43] derived from Skyrme energy-density functionals, dramatically underpredict data. Calculations using covariant density-functional theory and a five-dimensional collective Hamiltonian [44] predict a smooth, gradual prolate-triaxial transition across the W isotopic chain with an intermediate γ-soft minimum occurring at ^{190}W, but an oblate minimum does not develop thereafter. This cross-over transition is reflected by a slow, gradual change of calculated spectroscopic quadrupole moments from negative (prolate) values to about zero, where ^{190}W is predicted to have a quadrupole moment of about $Q_s = -1.1$ eb. This is contrary to the γ-soft limiting value of $Q_s = 0$ eb. The calculated $B(E2)$ values from these calculations significantly overpredict data, with a too steep negative slope toward large N, which is not favored by data. An approach based on the Gogny-D1M energy density functional [42] and an IBM-mapping procedure (EDF-IBM-2) [32] is consistent with a γ-soft structure of ^{190}W and the development of oblate deformation beyond $N = 116$, as it has been observed in data across the broader region [3]. In the following, we will adopt and further develop the latter approach and compare data to the predictions of the EDF-IBM-2 model for the W isotopic chain.

For a shape (phase) transition from prolate to oblate nuclei, one would naively expect a minimum $B(E2)$ value closest to the γ-soft limit and a rise when entering an oblate-deformed region, if the absolute value of quadrupole deformation β would stay constant. This would correspond to a switch of the spectroscopic quadrupole moment of the 2_1^+ state from negative to positive values, crossing zero at the γ-soft limit. In schematic IBM-1 calculations with constant boson numbers N this is reflected by a mirror (point) symmetry of the $B(E2)$ (Q) values with respect to $\chi = 0$, corresponding to $\gamma = 30°$ as seen, e.g., in Ref. [3]. However, one must take into account the shrinking valence space when approaching the major shell closure at $N = 126$, which impacts the degree of collectivity and, hence, will alter the trend.

For details on the calculation of spectroscopic properties of tungsten isotopes, we refer to Ref. [32]. Based on the Gogny-D1M energy density functional, a Hartree-Fock-Boguliubov (HFB) calculation yielded a potential energy surface (PES) for each isotope. Similarly, PES can be calculated using the IBM-2, and its parameters are fitted to derive a maximum overlap of both, the HFB and the IBM-2 PES. The details of this mapping procedure are found in Refs. [59–61]. Then, the IBM-2 calculations yield the low-energy spectrum of each respective isotope, as well as the $E2$ matrix elements. However, we point out that in this procedure it is not possible to fit effective charges isotope by isotope, and in [32] a constant value had been used.

In Fig. 7(b) we compare the $B(E2)$ data on W isotopes, up to ^{190}W, to the calculated values using the same effective charges as in Ref. [32] (EDF-IBM-2). One observes that the previous prediction from Ref. [32] underestimates, systematically, all $B(E2)$ values. While the absolute scale of $B(E2)$ values can simply be set by adjusting the effective boson charge in the model, the slope, which turned out to be too steep in the calculations from [32], is more difficult to obtain. We followed two alternative approaches to try to resolve this situation.

Our first approach is inspired by the work of Casten and Wolf [62], introducing boson-number dependent effective charges. In the original EDF-IBM2 description [32] a common effective charge of $e_B = e_\nu = e_\pi = 0.13$ eb had been used. We rescaled the effective boson charge to $\tilde{e}_B = 0.5(1 + 0.15\chi)((N + 1)/N)e_B$ with $\chi = 0.5(\chi_\pi + \chi_\nu)$ and $e_B = 0.27$ eb. The resulting values are shown in Fig. 7(b) labeled as "EDF-IBM2-N", reproducing the known data well, but resulting in a seemingly high $B(E2)$ value of almost 60 W.u. for the heaviest calculated isotope, ^{196}W. We note that this approach involves two parameters - an effective boson charge e_B and a slope for the χ dependence, which has been obtained within the IBM in Ref. [62], but which is adjusted to data in our approach while maintaining a boson charge e_B typically found in this region.

The second approach uses different effective charges for protons and neutrons, e_π and e_ν. To describe the available data well on average

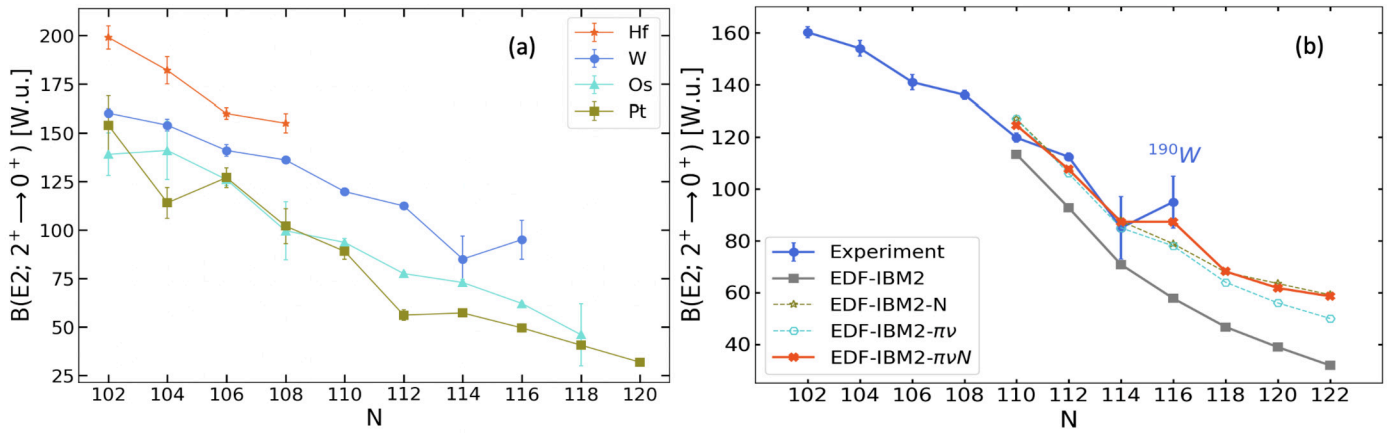

Fig. 7. (a) Experimental $B(E2;2_1^+ \to 0_1^+)$ values in even-even Hf, W, Os, Pt isotopes. The literature data was taken from Refs. [8–22]. (b) Comparison of experimental and theory $B(E2;2_1^+ \to 0_1^+)$ values for even-even tungsten isotopes.

we used a fixed ratio of $e_\pi/e_\nu = 1.5$, which led to the best description of data and derived $e_\nu = 0.122$ eb $e_\pi = 0.183$ eb. The resulting $B(E2)$ values from this calculation are also included in Fig. 7(b), labeled as "EDF-IBM2-$\pi\nu$". Using this approach, the systematic trend of data is better reproduced, similar to the EDF-IBM2-N method. In particular, besides the absolute scale, the slope of decreasing calculated $B(E2)$ values changed in the vicinity of known data, but drops somewhat faster toward the $N = 126$ shell closure than the boson-number dependent approach.

With the first approach described above reflecting the dependence of the $B(E2)$ values on the size of the valence space and degree of axial symmetry, and the second reflecting the difference in proton and neutron effective charges, both have well-founded origins. Therefore, we finally combined both in order to obtain a calculation taking all of these effects into account. That is, the proton effective charge has been fixed to $e_\pi = 0.2175$ eb, and a neutron effective charge to $e_\nu = 0.1450$ eb, so that the ratio of 1.5 holds. The neutron effective charge was allowed to vary with neutron-boson number N_ν and χ_ν as $\tilde{e}_\nu = 0.5\,(1 - 0.3\,\chi_\nu)\,((N_\nu + 1)/N_\nu)\,e_\nu$.

The results from this combined approach are labeled as "EDF-IBM2-$\pi\nu$N" in Fig. 7(b), and give the best overall agreement with data up to ^{190}W. It is noteworthy to point out the flat behavior of $B(E2)$ values between ^{188}W and ^{190}W in the calculation, which is due to the change of sign in χ_ν, as a consequence of the transition from prolate to oblate deformation. This trend is only tentatively indicated by the W data due to the large uncertainties at neutron numbers 114 and 116. Extending the EDF-IBM-2-$\pi\nu$N would be of high interest, but requires extended EDF-IBM-2 calculations toward lower neutron numbers, and would strongly benefit from more precise measurements of the ^{188}W and ^{190}W $B(E2)$ values.

The continuous drop of $B(E2)$ values beyond $N = 116$ seemingly contradicts the schematic expectation for a rise from the γ-soft limit toward oblate well-deformed isotopes. Therefore, we also show the calculated spectroscopic quadrupole moments, $Q_s(2_1^+)$ in Fig. 8. One observes the expected flip from negative to positive values from $N = 114$ to $N = 116$, indicating the proximity to the prolate-oblate phase transition. However, we note that the absolute values on the oblate side are smaller. The reason for this behavior is the approach of the $N = 126$ shell closure. In the IBM-2, this is reflected in the decrease in the number of (neutron) bosons, which directly enters the calculation of $E2$ matrix elements. Therefore, despite the switch from prolate to oblate deformation at ^{190}W, a continuous drop of $B(E2)$ values is predicted, in good agreement with the observed trend in the experiment. From these considerations, in view of the systematical behavior of the $R_{4/2}$, B_{22} and $B(E2)$ values, the spectroscopic data on ^{190}W matches the predictions for the most γ-soft, $O(6)$-like, isotope in the W isotopic chain, approaching the $N = 126$ shell closure.

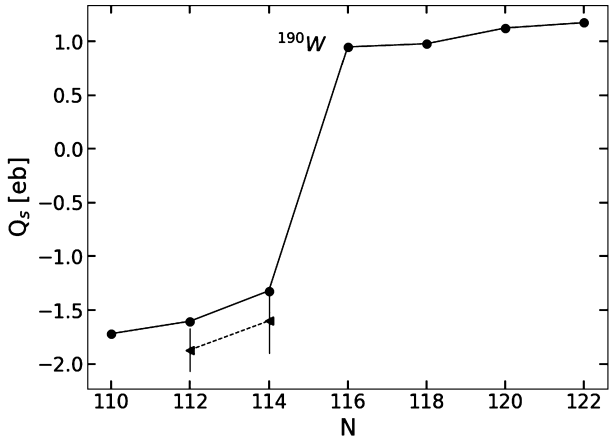

Fig. 8. Spectroscopic quadrupole moments Q_s for W isotopes as calculated in the EDF-IBM2-$\pi\nu$N approach (circles). In addition, the two available data points [8,13] at $N = 112, 114$ are shown (triangle) with their uncertainties.

4. Summary

In summary, the current measurement has determined the mean lifetime of the first 2^+ state of ^{190}W to 274(28) ps, which results in a $B(E2;2_1^+ \to 0_1^+)$ value of 95(10) W.u. This value indicates a halt in the decreasing trend of $B(E2)$ values in the W isotopic chain, and is in line with the expectations from revised EDF-IBM-2 calculations, taking into account effects of axial symmetry, size of the valence space, and the proton-neutron degree of freedom. The calculations clearly indicate the switch from prolate to oblate deformation, while collectivity overall decreases due to the approach of the $N = 126$ shell closure.

Declaration of competing interest

The authors declare that they have no known competing financial interests or personal relationships that could have appeared to influence the work reported in this paper.

Data availability

Data will be made available on request.

Acknowledgements

We would like to acknowledge the excellent work of the GSI accelerator department. E.Ş., V.W., A.K.M., U.A., and N.H. acknowledge support by the Helmholtz Research Academy Hesse for FAIR

(HFHF) and funds for cooperation between TU Darmstadt and GSI. J.J., A.B., A.E., V.K., P.K., L.K., V.W. acknowledge support by the BMBF-Rahmenprogramm ErUM Verbundsprojekt ErUM-FSP T07 grant nos. 05P19PKFNA, 05P21RDFNA, 05P21RDFN1, 05P19RDFN1, and 05P21PKFN1. P.H.R., Z.P. and M.M.R.C. were supported by the UK Nuclear Data Network and the UK STFC via Grant Nos. ST/L005743/1 and ST/P005314, P.H.R. acknowledges support from the UK Government Department of Business, Energy, and Industrial Strategy via the National Measurement System. R.L., M.S., G.H. acknowledge support by IN2P3-GSI collaboration agreements 18-78 France on GSI/FAIR. This work was supported by the Swedish Research Council under Grant Nos. 621-2014-5558 and 2019-04880. J.B, L.M.F., M.L.-E., and J.R.M. acknowledge funding through the Spanish government via project number RTI2018-098868-B-I00. Work at JSI was supported by the Slovenian Research Agency Grant Nos. I0-0005 and P1-0102. A.Z. was supported by the Hellenic Foundation for Research and Innovation (HFRI) under the HFRI PhD Fellowship grant (Fellowship Number: 101742/2019). B.S.N.S would like to acknowledge the financial support of the UKRI STFC through Grant Nos. ST/T001739/1 and ST/P005101/1. Funding by the European Commission H2020 Framework Programme project ENSAR2 (Grant agreement ID: 654002) is acknowledged. P.-A.S. acknowledges the support of the Romanian Ministry of Research and Innovation under research contract PN 23 21 01 06. This work was supported by the Basic Science Research Program through the National Research Foundation of Korea (NRF) funded by the Ministry of Education, grant no. 2020R1A6A3A03039081. Financial support from PRIN2017 project 2017P8KMFT CTADIR from the Italian Ministry of Education, University and Research is acknowledged. The results presented here are based on the experiment S452, which was performed at the target station S4 at the GSI Helmholtzzentrum fuer Schwerionenforschung, Darmstadt, Germany in the frame of FAIR Phase-0.

References

[1] W. Nazarewicz, M. Riley, J. Garrett, Equilibrium deformations and excitation energies of single-quasiproton band heads of rare-Earth nuclei, Nucl. Phys. A 512 (1) (1990) 61–96, https://doi.org/10.1016/0375-9474(90)90004-6.
[2] R. Bengtsson, T. Bengtsson, J. Dudek, G. Leander, W. Nazarewicz, J. ye Zhang, Shape coexistence and shape transitions in even-even Pt and Hg isotopes, Phys. Lett. B 183 (1) (1987) 1–6, https://doi.org/10.1016/0370-2693(87)91406-7.
[3] J. Jolie, A. Linnemann, Prolate-oblate phase transition in the Hf-Hg mass region, Phys. Rev. C 68 (2003) 031301, https://doi.org/10.1103/PhysRevC.68.031301.
[4] P.D. Stevenson, M.P. Brine, Zs. Podolyák, P.H. Regan, P.M. Walker, J. Rikovska Stone, Shape evolution in the neutron-rich tungsten region, Phys. Rev. C 72 (2005) 047303, https://doi.org/10.1103/PhysRevC.72.047303.
[5] P. Sarriguren, R. Rodríguez-Guzmán, L.M. Robledo, Shape transitions in neutron-rich Yb, Hf, W, Os, and Pt isotopes within a Skyrme Hartree-Fock+ BCS approach, Phys. Rev. C 77 (2008) 064322, https://doi.org/10.1103/PhysRevC.77.064322.
[6] R.F. Casten, Nuclear Structure from a Simple Perspective, vol. 23, Oxford University Press on Demand, 2000.
[7] R.F. Casten, B.M. Sherrill, The study of exotic nuclei, Prog. Part. Nucl. Phys. 45 (2000) S171–S233, https://doi.org/10.1016/S0146-6410(00)90013-9.
[8] J.C. Batchelder, A.M. Hurst, M.S. Basunia, Nuclear data sheets for A = 186, Nucl. Data Sheets 183 (1) (2022) 1–346, https://doi.org/10.1016/j.nds.2022.06.001.
[9] B. Singh, Nuclear data sheets for A = 190, Nucl. Data Sheets 99 (2) (2003) 275–481, https://doi.org/10.1006/ndsh.2003.0009.
[10] E. Achterberg, O.A. Capurro, G.V. Marti, Nuclear data sheets for A = 178, Nucl. Data Sheets 110 (7) (2009) 1473–1688, https://doi.org/10.1016/j.nds.2009.05.002.
[11] S.-C. Wu, H. Niu, Nuclear data sheets for A = 180, Nucl. Data Sheets 100 (4) (2003) 483–705, https://doi.org/10.1006/ndsh.2003.0018.
[12] B. Singh, J.C. Roediger, Nuclear data sheets for A = 182, Nucl. Data Sheets 111 (8) (2010) 2081–2330, https://doi.org/10.1016/j.nds.2010.08.001.
[13] C.M. Baglin, Nuclear data sheets for A = 184, Nucl. Data Sheets 111 (2) (2010) 275–523, https://doi.org/10.1016/j.nds.2010.01.001.
[14] B. Singh, Nuclear data sheets for A = 188, Nucl. Data Sheets 95 (2) (2002) 387–541, https://doi.org/10.1006/ndsh.2002.0005.
[15] E. Browne, H. Junde, Nuclear data sheets for A = 174, Nucl. Data Sheets 87 (1) (1999) 15–176, https://doi.org/10.1006/ndsh.1999.0015.
[16] M. Basunia, Nuclear data sheets for A = 176, Nucl. Data Sheets 107 (4) (2006) 791–1026, https://doi.org/10.1016/j.nds.2006.03.001.
[17] C.M. Baglin, Nuclear data sheets for A = 192, Nucl. Data Sheets 84 (4) (1998) 717–900, https://doi.org/10.1006/ndsh.1998.0017.
[18] B. Singh, Nuclear data sheets for A = 194, Nucl. Data Sheets 107 (6) (2006) 1531–1746, https://doi.org/10.1016/j.nds.2006.05.004.
[19] H. Xiaolong, Nuclear data sheets for A = 196, Nucl. Data Sheets 108 (6) (2007) 1093–1286, https://doi.org/10.1016/j.nds.2007.05.001.
[20] H. Xiaolong, Nuclear data sheets for A = 198, Nucl. Data Sheets 110 (10) (2009) 2533–2688, https://doi.org/10.1016/j.nds.2009.09.002.
[21] J.-M. Régis, T. Materna, S. Christen, C. Bernards, N. Braun, G. Breuer, C. Fransen, S. Heinze, J. Jolie, T. Meersschaut, G. Pascovici, M. Rudigier, L. Steinert, S. Thiel, N. Warr, K. Zell, Sub-nanosecond lifetime measurements using the double orange spectrometer at the cologne 10 MV Tandem accelerator, Nucl. Instrum. Methods Phys. Res., Sect. A, Accel. Spectrom. Detect. Assoc. Equip. 606 (3) (2009) 466–474, https://doi.org/10.1016/j.nima.2009.04.008.
[22] M. Rudigier, J.-M. Régis, J. Jolie, K. Zell, C. Fransen, Lifetime of the first excited 2^+ state in ^{172}W and ^{178}W, Nucl. Phys. A 847 (1) (2010) 89–100, https://doi.org/10.1016/j.nuclphysa.2010.07.003.
[23] D. Warner, A triple point in nuclei, Nature 420 (6916) (2002) 614–615, https://doi.org/10.1038/420614a.
[24] F. Iachello, Analytic description of critical point nuclei in a spherical-axially deformed shape phase transition, Phys. Rev. Lett. 87 (2001) 052502, https://doi.org/10.1103/PhysRevLett.87.052502.
[25] R.F. Casten, N.V. Zamfir, Empirical realization of a critical point description in atomic nuclei, Phys. Rev. Lett. 87 (2001) 052503, https://doi.org/10.1103/PhysRevLett.87.052503.
[26] N. Pietralla, O.M. Gorbachenko, Evolution of the "β excitation" in axially symmetric transitional nuclei, Phys. Rev. C 70 (2004) 011304, https://doi.org/10.1103/PhysRevC.70.011304.
[27] J. Jolie, P. Cejnar, R.F. Casten, S. Heinze, A. Linnemann, V. Werner, Triple point of nuclear deformations, Phys. Rev. Lett. 89 (2002) 182502, https://doi.org/10.1103/PhysRevLett.89.182502.
[28] T. Shizuma, T. Ishii, H. Makii, T. Hayakawa, S. Shigematsu, M. Matsuda, E. Ideguchi, Y. Zheng, M. Liu, T. Morikawa, et al., Excited states in neutron-rich ^{188}W produced by an ^{18}O induced 2-neutron transfer reaction, Eur. Phys. J. A, Hadrons Nucl. 30 (2) (2006) 391–396, https://doi.org/10.1140/epja/i2006-10139-0.
[29] N. Alkhomashi, P. Regan, Zs. Podolyák, S. Pietri, A.B. Garnsworthy, S.J. Steer, J. Benlliure, E. Caserejos, R.F. Casten, J. Gerl, et al., β^--delayed spectroscopy of neutron-rich tantalum nuclei: shape evolution in neutron-rich tungsten isotopes, Phys. Rev. C 80 (2009) 064308, https://doi.org/10.1103/PhysRevC.80.064308.
[30] G.J. Lane, G.D. Dracoulis, F.G. Kondev, R.O. Hughes, H. Watanabe, A.P. Byrne, M.P. Carpenter, C.J. Chiara, P. Chowdhury, R.V.F. Janssens, T. Lauritsen, C.J. Lister, E.A. McCutchan, D. Seweryniak, I. Stefanescu, S. Zhu, Structure of neutron-rich tungsten nuclei and evidence for a 10^- isomer in ^{190}W, Phys. Rev. C 82 (2010) 051304, https://doi.org/10.1103/PhysRevC.82.051304.
[31] C. Wheldon, J. Garcés Narro, C.J. Pearson, P.H. Regan, Zs. Podolyák, D.D. Warner, P. Fallon, A.O. Macchiavelli, M. Cromaz, Yrast states in ^{194}Os: the prolate-oblate transition region, Phys. Rev. C 63 (2000) 011304, https://doi.org/10.1103/PhysRevC.63.011304.
[32] K. Nomura, T. Otsuka, R. Rodríguez-Guzmán, L.M. Robledo, P. Sarriguren, Collective structural evolution in neutron-rich Yb, Hf, W, Os, and Pt isotopes, Phys. Rev. C 84 (2011) 054316, https://doi.org/10.1103/PhysRevC.84.054316.
[33] K. Nomura, T. Otsuka, R. Rodríguez-Guzmán, L.M. Robledo, P. Sarriguren, P.H. Regan, P.D. Stevenson, Zs. Podolyák, Spectroscopic calculations of the low-lying structure in exotic Os and W isotopes, Phys. Rev. C 83 (2011) 054303, https://doi.org/10.1103/PhysRevC.83.054303.
[34] Zs. Podolyák, P.H. Regan, M. Pfützner, J. Gerl, M. Hellström, M.C. no, P. Mayet, C. Schlegel, A. Aprahamian, J. Benlliure, A.M. Bruce, P.A. Butler, D.C. Gil, D.M. Cullen, J. Döring, T. Enqvist, F. Rejmund, C. Fox, J.G. Narro, H. Geissel, W. Gelletly, J. Giovinazzo, M. Górska, H. Grawe, R. Grzywacz, A. Kleinböhl, W. Korten, M. Lewitowicz, R. Lucas, H. Mach, M. Sawicka, H. Schaffner, K. Schmidt, C. Theisen, P.M. Walker, D.D. Warner, C. Wheldon, H.J. Wollersheim, S.C. Wooding, F.R. Xu, Isomer spectroscopy of neutron rich $^{190}W_{116}$, Phys. Lett. B 491 (3–4) (2000) 225, https://doi.org/10.1016/S0370-2693(00)01051-0.
[35] J.A. Cizewski, R.F. Casten, G.J. Smith, M.L. Stelts, W.R. Kane, H.G. Börner, W.F. Davidson, Evidence for a new symmetry in nuclei: the structure of Pt 196 and the O(6) limit, Phys. Rev. Lett. 40 (3) (1978) 167, https://doi.org/10.1103/PhysRevLett.40.167.
[36] R.F. Casten, P. von Brentano, K. Heyde, P. Van Isacker, J. Jolie, The interplay of γ-softness and triaxiality in O(6)-like nuclei, Nucl. Phys. A 439 (2) (1985) 289–298, https://doi.org/10.1016/0375-9474(85)90432-4.
[37] D. Cline, Nuclear shapes studied by Coulomb excitation, Annu. Rev. Nucl. Part. Sci. 36 (1) (1986) 683–716, https://doi.org/10.1146/annurev.ns.36.120186.003343.
[38] C.Y. Wu, D. Cline, T. Czosnyka, A. Backlin, C. Baktash, R.M. Diamond, G.D. Dracoulis, L. Hasselgren, H. Kluge, B. Kotlinski, et al., Quadrupole collectivity and shapes of Os Pt nuclei, Nucl. Phys. A 607 (2) (1996) 178–234, https://doi.org/10.1016/0375-9474(96)00181-9.
[39] V. Werner, C. Scholl, P. Von Brentano, Triaxiality and the determination of the cubic shape parameter K_3 from five observables, Phys. Rev. C 71 (5) (2005) 054314, https://doi.org/10.1103/PhysRevC.71.054314.
[40] Zs. Podolyák, Prolate-oblate shape transition in heavy neutron-rich nuclei, J. Phys. Conf. Ser. 381 (1) (2012) 012052, https://doi.org/10.1088/1742-6596/381/1/012052.
[41] P.J.R. Mason, Zs. Podolyák, N. Mărginean, P.H. Regan, P.D. Stevenson, V. Werner, T. Alexander, A. Algora, T. Alharbi, M. Bowry, et al., Half-life of the yrast 2^+ state

in ^{188}W: evolution of deformation and collectivity in neutron-rich tungsten isotopes, Phys. Rev. C 88 (2013) 044301, https://doi.org/10.1103/PhysRevC.88.044301.
[42] L.M. Robledo, R. Rodríguez-Guzmán, P. Sarriguren, Role of triaxiality in the ground-state shape of neutron-rich yb, hf, w, os and pt isotopes, J. Phys. G, Nucl. Part. Phys. 36 (2009) 115104, https://doi.org/10.1088/0954-3899/36/11/115104.
[43] M.T.S. Kannan, N. Ashok, S.S. Nayak, J. Sdhukhan, G. Mukherjee, Shape evolution of sub-lead neutron-rich nuclei around the neutron shell closure, Eur. Phys. J. A 59 (2023) 220, https://doi.org/10.1140/epja/s10050-023-01127-z.
[44] X.Q. Yang, L.J. Wang, J. Xiang, X.Y. Wu, Z.P. Li, Microscopic analysis of prolate-oblate shape phase transition and shape coexistence in the er-pt region, Phys. Rev. C 103 (2021) 054321, https://doi.org/10.1103/PhysRevC.103.054321.
[45] Q. Yang, H.-L. Wang, M.-L. Liu, F.-R. Xu, Characteristics of collectivity along the yrast line in even-even tungsten isotopes, Phys. Rev. C 94 (2016) 024310, https://doi.org/10.1103/PhysRevC.94.024310.
[46] A.K. Mistry, H.M. Albers, T. Arıcı, A. Banerjee, G. Benzoni, B. Cederwall, J. Gerl, M. Górska, O. Hall, N. Hubbard, et al., The DESPEC setup for GSI and FAIR, Nucl. Instrum. Methods Phys. Res., Sect. A, Accel. Spectrom. Detect. Assoc. Equip. 1033 (2022) 166662, https://doi.org/10.1016/j.nima.2022.166662.
[47] H. Geissel, P. Armbruster, K.H. Behr, A. Brünle, K. Burkard, M. Chen, H. Folger, B. Franczak, H. Keller, O. Klepper, et al., The GSI projectile fragment separator (FRS): a versatile magnetic system for relativistic heavy ions, Nucl. Instrum. Methods Phys. Res., Sect. B, Beam Interact. Mater. Atoms 70 (1) (1992) 286–297, https://doi.org/10.1016/0168-583X(92)95944-M.
[48] M.M.R. Chishti, S. Jazrawi, R. Shearman, P.H. Regan, Zs. Podolyák, S.M. Collins, M. Górska, B. Cederwall, A. Yaneva, G.X. Zhang, J. Cederkall, A. Goasduff, H.M. Albers, S. Alhomaidhi, A. Banerjee, A.M. Bruce, G. Benzoni, B. Das, T. Davinson, L.M. Fraile, J. Gerl, G. Häfner, J. Jolie, N. Hubbard, P.R. John, R. Lozeva, A.K. Mistry, B.S. Nara Singh, M. Mikolajczuk, M. Polettini, N. Pietralla, J.M. Regis, M. Rudigier, E. Sahin, A. Sharma, M. Si, J. Vesic, V. Werner, Response of the fasttiming array (fatima) for despec at fair phase-0, Nucl. Instrum. Methods Phys. Res., Sect. A 1056 (2023) 168597, https://doi.org/10.1016/j.nima.2023.168597.
[49] G.F. Farrelly, Zs. Podolyák, S.J. Steer, S. Pietri, F.R. Xu, E. Werner-Malento, T. Shizuma, P.H. Regan, D. Rudolph, A.B. Garnsworthy, R. Hoischen, M. Górska, J. Gerl, H.J. Wollersheim, T. Kurtukian-Nieto, G. Benzoni, F. Becker, P. Bednarczyk, L. Cáceres, Revision of the K-isomer in ^{190}W_116, Acta Phys. Pol. B 40 (3) (2009) 885, https://www.actaphys.uj.edu.pl/R/40/3/885/pdf.
[50] J.-M. Régis, M. Dannhoff, J. Jolie, A simple procedure for γ-γ lifetime measurements using multi-element fast-timing arrays, Nucl. Instrum. Methods Phys. Res., Sect. A, Accel. Spectrom. Detect. Assoc. Equip. 897 (2018) 38–46, https://doi.org/10.1016/j.nima.2018.04.047.
[51] J.-M. Régis, M. Dannhoff, J. Jolie, C. Müller-Gatermann, N. Saed-Samii, On the time response of background obtained in γ-ray spectroscopy experiments using $LaBr_3$(Ce) detectors with different shielding, Nucl. Instrum. Methods Phys. Res., Sect. A, Accel. Spectrom. Detect. Assoc. Equip. 811 (2016) 42–48, https://doi.org/10.1016/j.nima.2015.12.017.
[52] Z. Bay, Calculation of decay times from coincidence experiments, Phys. Rev. 77 (1950) 419, https://doi.org/10.1103/PhysRev.77.419.
[53] J.-M. Régis, J. Jolie, H. Mach, G.S. Simpson, A. Blazhev, G. Pascovici, M. Pfeiffer, M. Rudigier, N. Saed-Samii, N. Warr, et al., The generalized centroid difference method for lifetime measurements via γ-γ coincidences using large fast-timing arrays, EPJ Web Conf. 93 (2015) 01013, https://doi.org/10.1051/epjconf/20159301013.
[54] W.D. Hamilton, Electromagnetic Interaction in Nuclear Spectroscopy, North-Holland Publishing Co., Amsterdam, 1975.
[55] J.-M. Régis, G. Pascovici, J. Jolie, M. Rudigier, The mirror symmetric centroid difference method for picosecond lifetime measurements via γ–γ coincidences using very fast $LaBr_3$(Ce) scintillator detectors, Nucl. Instrum. Methods Phys. Res., Sect. A, Accel. Spectrom. Detect. Assoc. Equip. 622 (1) (2010) 83–92, https://doi.org/10.1016/j.nima.2010.07.047.
[56] J.-M. Régis, H. Mach, G.S. Simpson, J. Jolie, G. Pascovici, N. Saed-Samii, N. Warr, A. Bruce, J. Degenkolb, L.M. Fraile, et al., The generalized centroid difference method for picosecond sensitive determination of lifetimes of nuclear excited states using large fast-timing arrays, Nucl. Instrum. Methods Phys. Res., Sect. A, Accel. Spectrom. Detect. Assoc. Equip. 726 (2013) 191–202, https://doi.org/10.1016/j.nima.2013.05.126.
[57] T. Kibédi, T.W. Burrows, M.B. Trzhaskovskaya, P.M. Davidson, C.W. Nestor Jr., Evaluation of theoretical conversion coefficients using bricc, Nucl. Instrum. Methods Phys. Res., Sect. A, Accel. Spectrom. Detect. Assoc. Equip. 589 (2008) 202, https://doi.org/10.1016/j.nima.2008.02.051.
[58] F. Iachello, A. Arima, The Interacting Boson Model, Cambridge University Press, Cambridge, 1987.
[59] K. Nomura, N. Shimizu, T. Otsuka, Mean-field derivation of the interacting boson model Hamiltonian and exotic nuclei, Phys. Rev. Lett. 101 (2008) 142501, https://doi.org/10.1103/PhysRevLett.101.142501.
[60] K. Nomura, N. Shimizu, T. Otsuka, Formulating the interacting boson model by mean-field methods, Phys. Rev. C 81 (2010) 044307, https://doi.org/10.1103/PhysRevC.81.044307.
[61] K. Nomura, T. Otsuka, N. Shimizu, L. Guo, Microscopic formulation of the interacting boson model for rotational nuclei, Phys. Rev. C 83 (2011) 041302(R), https://doi.org/10.1103/PhysRevC.83.041302.
[62] R.F. Casten, A. Wolf, Approximate analytic expression for B(E2) values in the interacting boson model, Phys. Rev. C 35 (3) (1987) 1156, https://doi.org/10.1103/PhysRevC.35.1156.